THE ASTROPHYSICAL JOURNAL, 552:42–48, 2001 May 1

EXTENDED SUNYAEV-ZELDOVICH MAP OF THE MOST LUMINOUS X-RAY CLUSTER, RX J1347−1145

E. POINTECOUTEAU AND M. GIARD
Centre d'Etude Spatiale des Rayonnements, 9 avenue du colonel Roche, BP4346, F-31028 Toulouse Cedex 4, France; pointeco@cesr.fr
A. BENOIT
Centre de Recherche des Très Basses Températures, 25 avenue des Martyrs, BP 166, F-38042 Grenoble Cedex 9, France
F. X. DÉSERT
Laboratoire d'Astrophysique de l'Observatoire de Grenoble, 414 rue de la Piscine, F-38041 Grenoble Cedex 9, France
AND
J. P. BERNARD, N. CORON, AND J. M. LAMARRE
Institut d'Astrophysique Spatiale, Bât 121, Université Paris-Sud, F-91405 Orsay Cedex, France
Received 2000 September 18; accepted 2000 December 14

ABSTRACT

We present a high-resolution (22″ FWHM) extended map at 2.1 mm of the Sunyaev-Zeldovich effect toward the most luminous X-ray cluster, RX J1347−1145. These observations have been performed with the Diabolo photometer working at the focus of the 30 m IRAM radiotelescope. We have derived a projected gas mass of $(1.1 \pm 0.1) \times 10^{14}\ h_{50}^{-5/2}\ M_{\odot}$ within an angular radius of $\theta = 74''$ (i.e., projected radius of 0.6 Mpc, $H_0 = 50$ km s^{-1} Mpc^{-1}, $\Omega_m = 0.3$, $\Omega_\Lambda = 0.7$). This result matches very well the expected gas mass from the cluster models of X-ray data. With an unprecedented sensitivity level, our measurement does not show significant departure from a spherical distribution. The data analysis also allows us to characterize the 2.1 mm flux of a well-known radio source lying in the center of the cluster, $F_{\rm RS}(2.1\ {\rm mm}) = 5.7 \pm 1.6$ mJy.

Subject headings: cosmic microwave background — cosmology: observations — galaxies: clusters: individual (RX J1347−1145) — intergalactic medium

1. INTRODUCTION

The statistical properties of galaxy clusters (shape, structures, size, temperature, mass) depend strongly on the geometry of the universe. Studying them provides some robust constraints on cosmological models, structure formation, and evolution (Oukbir, Bartlett, & Blanchard 1997; Sadat, Blanchard, & Oukbir 1998; Bahcall & Fan 1998). This strong coupling makes the study of massive and distant clusters a very useful tool for cosmology. The intergalactic gas component can be observed through its Bremsstrahlung emission at X-ray wavelengths. It can also be detected from submillimeter to radio wavelengths via the Sunyaev-Zeldovich (SZ) effect (Sunyaev & Zeldovich 1972). Whereas the X-ray emission depends on the square of the gas density, the SZ effect is linearly dependent on this quantity. For this reason, the SZ effect is proportional to the column density and thus to the line-of-sight integrated gas mass. Moreover, the SZ signal does not suffer from the brightness decrease of radiation (in particular the X-ray) due to the expansion of the universe (see the review by Birkinshaw 1999).

The RX J1347−1145 cluster is known as the most luminous X-ray cluster to date. It has been detected in the *ROSAT* All-Sky Survey and further studied with the *ROSAT* HRI and the *ASCA* GIS2 instruments (Schindler et al. 1995, 1997). With an intrinsic bolometric X-ray luminosity of $L_{\rm bol} = 21 \times 10^{45}\ h_{50}^{-2}$ ergs s^{-1}, it shows a very peaked X-ray emission profile with an angular core radius of $\theta_c = 8\farcs4 \pm 1\farcs8$. It also presents a very strong cooling flow in its central region, with a corresponding accreting rate of $\dot{M}_{\rm cool} = 3000\ M_{\odot}\ {\rm yr}^{-1}$. It is a distant cluster with $z = 0.45$, so that the angular distance is $1670\ h_{50}^{-1}$ Mpc (490 pc arcmin^{-1}, with $H_0 = 50$km s^{-1} Mpc^{-1}, $\Omega_m = 0.3$, $\Omega_\Lambda = 0.7$; 410 pc arcmin^{-1} in a standard CDM model). The value of the core radius with these two sets of cosmological parameters is respectively equal to 68 kpc (ΛCDM model) and 57 kpc (standard CDM model). The total binding mass derived from the X-ray data within 1 Mpc is $M_{\rm tot} = 5.8 \times 10^{14}\ h_{50}^{-1}\ M_{\odot}$. This value is to be compared to those obtained from the optical gravitational lensing follow-up achieved by Fischer & Tyson (1997) and Sahu et al. (1998). Within the same radius, they provide a value of $M_{\rm tot} = 1.7 \times 10^{15}\ h_{50}^{-1}\ M_{\odot}$ (Fischer & Tyson 1997).

In a previous paper, we reported the detection of a very strong SZ effect in the direction of RX J1347−1145 with the Diabolo photometer (Pointecouteau et al. 1999). We presented a map of the cluster central region (2′ × 1′). The corresponding Comptonization parameter was $y(0) = 12.7^{+2.9}_{-3.1} \times 10^{-4}$ (1 σ error bars). During the 1999 Diabolo run, we performed an extended mapping of RX J1347−1145 over a 4′ by 4′ field. The size of the first map was rather small, so that only a one-dimensional average slice was used to compare with the X-ray data. Here the size of the map allows us to make full use of two-dimensional information on the cluster. Moreover, the computation of a cluster radial profile from a two-dimensional map allows us to discard most of the effects induced by point sources.

In this paper we present the resulting extended map of this cluster at 2.1 mm. In § 2, we detail the observation procedures and characteristics. In § 3 we describe the data processing, and in § 4 we analyze the astrophysical data. Finally, in § 5 we discuss the results. Throughout this paper, we use the following values for the cosmological parameters: $H_0 = 50\ {\rm km\ s^{-1}\ Mpc^{-1}}$, $\Omega_m = 0.3$, $\Omega_\Lambda = 0.7$.

2. OBSERVATIONS

The Diabolo instrument is a dual-channel photometer working at 1.2 and 2.1 mm. The detectors are bolometers

cooled down to 0.1 K using an open cycle ^{4}He–^{3}He dilution refrigerator (Benoit et al. 2000). Two thermometers associated with a heater and a PID digital control system are used to regulate the temperature of the 0.1 K plate. There are three adjacent bolometers per channel, arranged in an equilateral triangle at the focus of the telescope. For a given channel, each bolometer is coaligned with one bolometer of the second channel, both looking toward the same sky direction. For the observations presented here, Diabolo was installed at the focus of the IRAM 30 m radio telescope at Pico Veleta (Spain). This configuration allows us to achieve a 22″ resolution at 2.1 mm. The 30 m telescope focus being of Nasmyth type, the rotation of the field must be taken into account in the reconstruction of the sky map. Désert et al. (1998) have described the experimental setup and reported the first Diabolo SZ detections.

RX J1347−1145 was observed in 1999 January for a total integration time of 17 hr. The X-ray emission center, $\alpha_{2000} = 13^h47^m31^s$, $\delta_{2000} = -11°45'11''$ (Schindler et al. 1997), has been taken as the map center. Each sequence of observation has been performed in the right ascension coordinates, using the Earth rotation as right ascension drift such that the telescope is kept fixed in local coordinates. The basic observation sequence was a 240″ × 240″ map in right ascension–declination coordinates, with a 10″ declination steps. The wobbling secondary mirror of the 30 m IRAM telescope has been used at a frequency of 1 Hz and with a modulation amplitude of 150″. The wobbling is horizontal (e.g., at constant elevation), thus not aligned with the scanning direction. In order to remove systematic signal drifts that are produced by the antenna environment, we used alternatively the positive and negative beam to map the cluster. We have produced 89 such maps.

3. DATA REDUCTION AND CALIBRATION

The data processing includes all the different steps described by Pointecouteau et al. (1999). This includes a correction from the cosmic-ray impacts, a synchronous demodulation of the signal, a subtraction of the atmospheric signal correlated between the two channels, a correction from the atmosphere opacity, a reprojection of each single observation on a final R.A.–decl. grid, a baseline subtraction supported by the edges of the map, and the computation of a final map at 1.2 and 2.1 mm by coadding the three bolometers of each channel. The beam modulation is performed with an amplitude of 150″, so that some of the "off" positions lie within the limit of our map. Consequently, the beam switching must be taken into account in the data analysis (see § 4.1).

Throughout the run, the pointing verifications have been performed in the direction of QSOs lying at about the same declination as the cluster. The planet Mars has been used as a calibration target and to map the beam pattern. Assuming that Mars is a point source with respect to Diabolo's beam (angular diameter around 5″ in 1999 January), the accuracy in the absolute calibration is better than 20% at 1.2 mm and 15% at 2.1 mm. Mars has been directly mapped in R.A.–decl. during this run. This method provides a direct view of the beam shape, and takes into account the eventual systematic effects, such as the beam elongation in the right-ascension direction due to the conjugated effects of the scanning drift speed and the bolometer time constant.

4. RESULTS AND DATA ANALYSIS

The reduced map for RX J1347−1145 at 2.1 mm is shown in Figure 1*a*. It has been smoothed using a Gaussian filter with 20″ FWHM. The contours overplotted correspond to 1, 2, 3, 4, and 5 σ detection levels (negative and positive contours are shown by solid and dashed lines, respectively). The noise level on this map is 1 mJy beam^{-1} in a 10″ × 10″ pixel (equivalent to 0.5 mJy beam^{-1} in the 22″ Diabolo beam and to 0.3 mJy beam^{-1} [equivalent to $y = 3 \times 10^{-5}$] in the 30″ FWHM effective beam after smoothing). This map exhibits a strong and extended SZ decrement in the direction of the cluster. Unfortunately, the Diabolo 1.2 mm data are very noisy. No positive SZ signal could be extract from them. We used them to subtract most of the atmospheric emission from the 2.1 mm data.

The signal does not seem to follow a symmetric circular distribution, as expected from the X-ray data and from the commonly used β-model. A first look at the map argues in favor of substructure in the signal, and so far, in the gas distribution. The X-ray map has been overplotted on the SZ map (see Fig. 1*c*). It has been computed from the whole *ROSAT* HRI observations (35 ks exposure time) obtained from the *ROSAT* database (the map published by Schindler et al. 1997 included only one-third of those data).

Since the SZ signal is linearly dependent on the gas density (scaled with n_e), the X-ray emission is dominated by contributions from regions of higher density (scaled with n_e^2). Furthermore, the X-ray and SZ signals are not sensitive to the same part of the gas. What appears as differences between the SZ and the X-ray spatial distributions could be associated with different gas phases with various physical states (density, pressure, temperature). In the following discussion, we compare in detail the measured SZ map to the expected SZ distribution deduced from the symmetrical cluster X-ray model.

4.1. *Modeling the SZ Signal*

From the *ROSAT* HRI X-ray map and the *ASCA* X-ray spectrum of RX J1347−1145, Schindler et al. (1995, 1997) have extracted the cluster physical parameters: $T_e = 9.3 \pm 0.5$ keV, $n_{e0} = 9.4 \times 10^{-3}$ cm^{-3}, $\theta_c = 8''.4 \pm 1''.8$, and $\beta = 0.56 \pm 0.04$ (1 σ errors), assuming a β-model for the gas distribution (Cavaliere & Fusco-Femiano 1976). Using those parameters, we can compute the Comptonization parameter expected toward the cluster center: $y_{\rm exp}(0) = (8.4 \pm 2.7) \times 10^{-4}\ h_{50}^{1/2}$. Following this approach, we used a β-model to describe our SZ signal. Because of the circular symmetry induced on the projected sky by this kind of model, we chose to test different β-models on the radial profile resulting from our 2.1 mm map (see Fig. 2). To model the SZ signal, we have taken into account the integration of the SZ spectrum on the Diabolo passbands and the integration of the gas distribution over the Diabolo beam shape. To perform a rigorous fit of the Diabolo data, we need to take into account in the model every step of the observing procedure and of the data-reduction procedure. Thus, whatever model we used, we considered it as a real sky and reproduced on it all the Diabolo observations performed in the direction of RX J1347-1147. (This includes the wobbling positions and amplitudes.) The resulting simulated data set of observations has been reduced in the same way as the real data set by following all steps of the Diabolo pipeline

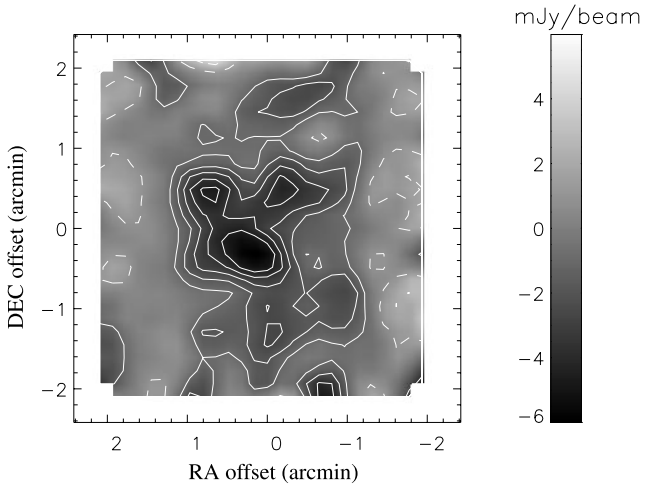

FIG. 1*a*

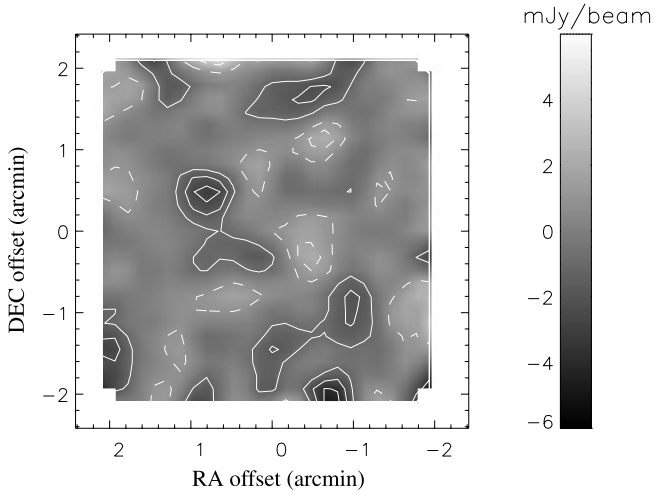

FIG. 1*b*

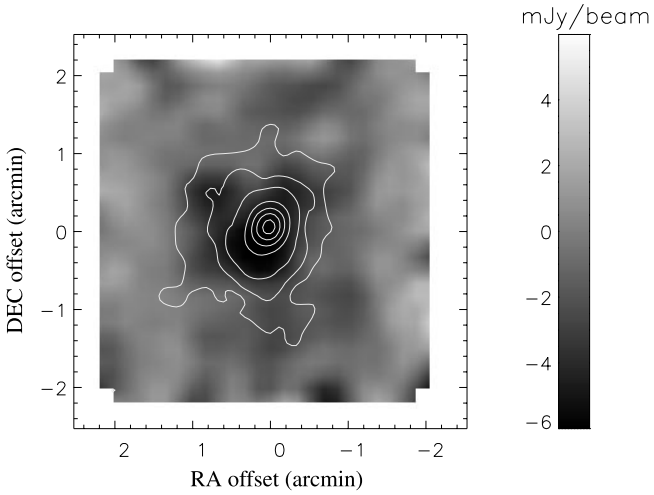

FIG. 1*c*

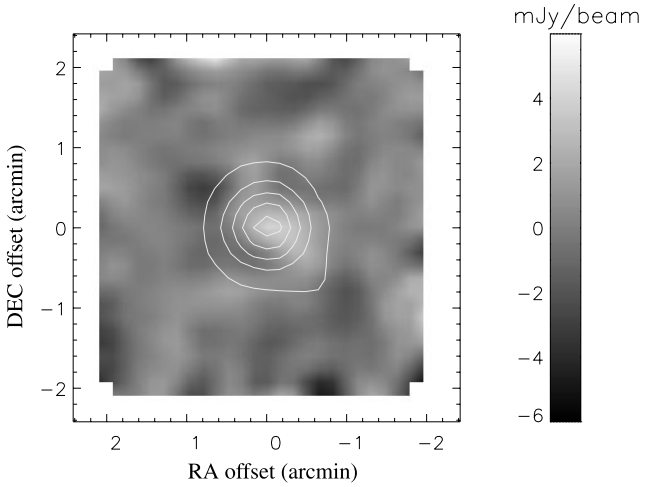

FIG. 1*d*

FIG. 1.—(*a*) 2.1 mm map of RX J1347−1145 obtained with the Diabolo photometer. This map and the three others have been smoothed by a Gaussian filter with 20″ FWHM. The 1 σ noise level in term of flux is 1 mJy in a pixel of 10″ × 10″ (equivalent to 0.5 mJy beam^{-1} in the 22′ Diabolo beam and to 0.3 mJy beam^{-1} in the 30″ FWHM effective beam after smoothing). (*b*) Residual map after subtraction of the best-fit model (SZ plus point source; see text). In the maps *a* and *b*, the overlying contours correspond to the 1, 2, 3, 4, and 5 σ detection levels. The negative and positive contours are shown by solid and dashed lines, respectively. (*c*) RX J1347−1145 SZ signal (after subtraction of the point-source best-fit model) compared to the X-ray cluster emission. The different contours overplotted correspond to 3%, 5%, 10%, 30%, 50%, 70%, and 90% of the X-ray maximum of emission. (*d*) Point-source detection at 2.1 mm after subtraction of the SZ best-fit model. The contours overlying correspond to the NVSS map (1%, 10%, 30%, 50%, 70%, and 90% of the radio maximum emission). The central position in the four map corresponds to the position of the X-ray center: $\alpha_{2000} = 13^{\rm h}47^{\rm m}31^{\rm s}$, $\delta_{2000} = -11°45'11''$.

(demodulation, base-line subtraction, reprojection, etc.; see § 3).

The resulting model for the flux of the SZ decrement per beam can be expressed as

$$F(\bar{\nu}, \mathbf{\Omega}) = y(0) \int \tau(\nu) \mathrm{SZ}(\nu, T_g) d\nu \int P(\mathbf{\Omega}) L(\mathbf{\Omega} - \mathbf{\Omega}') d\mathbf{\Omega}' \,, \quad (1)$$

where $y(0) = (k_{\rm B} T_g / m_e c^2) \sigma_{\rm T} \int n_e(l) dl$ is the Comptonization parameter toward the cluster center ($k_{\rm B}$ is the Boltzmann constant, m_e the electron mass, c the speed of light, $\sigma_{\rm T}$ is the Thomson cross section, and $n_e(l)$ is the electronic density along the line of sight). Here $\tau(\nu)$ is the normalized Diabolo band spectral efficiency, and $\mathrm{SZ}(\nu, T_g)$ represents the SZ spectrum. It is a numerical function of ν and T_g with a weak dependence on T_g that takes into account the relativistic corrections (Pointecouteau, Giard, & Barret 1998). The term $P(\mathbf{\Omega})$ represents the normalized gas profile projected on the sky and $L(\mathbf{\Omega})$ is the normalized Diabolo beam shape.

The cluster central region contains a radio point source, known from the NRAO VLA Sky Survey (NVSS; Condon et al. 1998), the coordinates of which are $\alpha_{2000} = 13^{\rm h}47^{\rm m}30\overset{\rm s}{.}7$ and $\delta_{2000} = -11°45'8\overset{''}{.}6$ (within the 3″ of the X-ray center). To avoid any contamination and bias of the SZ signal due to a residual millimeter emission of this radio point source, we chose to include its contribution in our model. We considered this source as a point source with respect to Diabolo's beam. This approach follows the method used by Pointecouteau et al. (1999):

$$F(\bar{\nu}, \mathbf{\Omega}) = F_{\rm RS}(\bar{\nu}) L(\mathbf{\Omega}) \,, \quad (2)$$

where $F_{\rm RS}(\bar{\nu})$ is the flux of the point source.

We have tested a total of five models with our data. Models A and B just include an SZ component. In model A, we choose the Comptonization parameter, the core radius, and β as free parameters. In model B, we just let y and r_c be free and fixed β to 0.56 (the X-ray value). The three other models are combinations of an SZ component and a point-

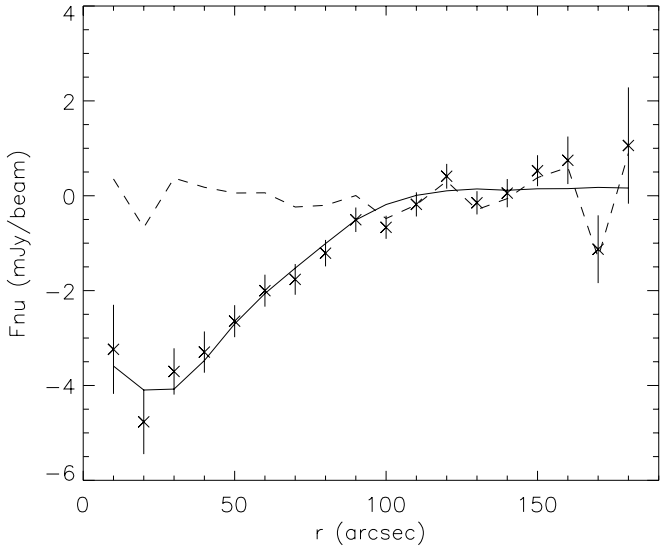

FIG. 2.—RX J1347−1145 radial profile at 2.1 mm computed from the Diabolo 2.1 mm map. The data point are plotted with their associated 1 σ error bars. The best-fit model (including an SZ component and a point-source component; see text) is overplotted (*solid line*). The residual radial profile is plotted as a dashed line.

source component. The parameters in model C are y, r_c, β, and F_{RS}. In model D, we let the y, r_c, and F_{RS} parameters be free ($\beta = 0.56$). Finally, for the E model, we have fixed the core radius and the β-parameter to their respective X-ray value of 8.″4 and 0.56. We used y and F_{RS} as free parameters. The models have been tested using a maximum-likelihood analysis method. The errors are obtained through the integration of the likelihood function over the parameter space. The best-fit parameters are gathered for the different cases in Table 1.

As shown by the results from models A and C, we cannot constraint the core radius and the β-parameter simultaneously, because those two parameters are too strongly coupled. For this reason, β has been fixed to the X-ray value of 0.56 in models B and D. Unfortunately, in those two cases the core radius also cannot be constrained precisely. Its determination suffers from a degeneracy, and despite the extent of our SZ map, we are not able to discriminate between a small and a high core radius model. This is a consequence of the way we have defined the zero level: a baseline subtraction in the R.A. direction fitted to 60% of the data points per line (30% on each edge). This operation is needed to eliminate the low-frequency detector noises. Consequently, whatever the model is, the cluster extension is cut off by the baseline subtraction, and the signal-to-noise ratio does not allow us to distinguish between a small and large core radius. For this reason, we have chosen to use the core radius value derived from the X-ray analysis, $\theta_c = 8.''4$, to describe the spatial gas distribution with a β-model. Following this hypothesis, we have adopted the model E as the best-fit model. The best-fit parameters are $y(0) = (7.9 \pm 0.5) \times 10^{-4}$ and $F_{RS} = 5.7 \pm 1.6$ mJy (with 68% confidence level error bars). In order to perform an accurate error analysis, we have also propagated the uncertainty on the X-ray parameter determination through the whole pipeline of the data analysis. The resulting 1 σ errors are $\Delta y = 1.1 \times 10^{-4}$ and $\Delta F_{RS} = 1.8$ mJy. Because we just use the information on the X-ray temperature to fix the exact shape of the SZ spectra (a second-order effect), the extra errors induced by the temperature uncertainty are marginally significant. The most important difference is driven by the core radius and by the β-parameter uncertainties. Figure 2 presents the best-fit radial profile model (SZ plus point-source signals) overlying the cluster radial profile as seen by Diabolo at 2.1 mm. The residual signal is overplotted as a dashed line.

TABLE 1

BEST-FIT PARAMETERS

Model	$y(0)$ (10^{-4})	θ_c (arcsec)	β	F_{RS} (mJy)	$\chi^2/(n-1)$[a]
A	$4.1^{+1.7}_{-0.4}$	$56.3^{+12.0}_{-19.1}$	$0.89^{+0.26}_{-0.61}$	0[b]	1.1
B	$5.3^{+0.8}_{-0.3}$	$32.4^{+18.4}_{-21.5}$	0.56[b]	0[b]	0.9
C	$5.7^{+0.3}_{-1.6}$	$12.4^{+40.2}_{-12.4}$	$0.51^{+0.34}_{-0.11}$	$3.4^{+2.6}_{-3.7}$	1.1
D	$5.7^{+0.4}_{-0.6}$	$14.8^{+28.7}_{-4.7}$	0.56[b]	$4.1^{+39.3}_{-5.9}$	0.9
E	$7.9^{+0.4}_{-0.5}$	8.4[b]	0.56[b]	$5.7^{+1.4}_{-1.6}$	1.1

[a] Where $(n-1)$ is the number of degrees of freedom.

[b] Fixed parameter; see text.

One can also perform a fit with y as a single free parameter. To do that, the central part of the map ($\theta_c < 30''$) is excluded from the radial profile computation. The best-fit parameter in this case is $y(0) = (7.8 \pm 0.4) \times 10^{-4}$. Afterward, the point-source flux can be derived from the residual map: $F_{RS} = 5.3 \pm 1.0$ mJy. Those two values are fully consistent with the previous ones. (The propagation of the X-ray parameter uncertainties reach to respective resulting errors of $\Delta y = 1.0 \times 10^{-4}$ and $\Delta F_\nu = 1.2$ mJy.) Our y-value is in very good agreement within a 68% confidence level with the value expected from X-ray data. Moreover, it is in very good agreement with the value determined by Komatsu et al. (2001) from their 21 GHz data: $y(0) = (7.7 \pm 1.6) \times 10^{-4}$. Finally, within the 2 σ of our previous determination, $y(0) = 12.7^{+2.9}_{-3.1} \times 10^{-4}$ (Pointecouteau et al. 1999). Combining the $y(0)$ value expected from the X-ray data [$y_{exp}(0) = (8.4 \pm 2.7) \times 10^{-4} h_{50}^{1/2}$] and the one we estimated from our SZ measurements, we are able to derived the H_0 value: $H_0 = 44 \pm 6$ km s^{-1} Mpc^{-1}. The error quoted on H_0 just includes the uncertainty on our $y(0)$ determination. If the uncertainties on the X-ray parameters are taken into account, the error on H_0 become ± 15 km s^{-1} Mpc^{-1}. Obviously, this does not take into account any other uncertainty or any systematic errors due to the cluster geometry or to the hypothesis concerning the gas isothermality or the hydrostatic equilibrium.

The residual signal resulting from the data map and the best-fit model map difference is presented in Figure 1*b* (where a Gaussian 20″ FWHM filtering has been performed). The 1, 2, and 3 σ detection levels have been overplotted (*solid contours for the negative signal*). This map is mostly compatible with noise, the higher deviation being a decrement (-3.1 ± 0.9 mJy) located to the northeast of the cluster center ($\Delta\alpha = +35''$, $\Delta\delta = +30''$), with a significance 3.5 σ.

Komatsu et al. (2001) have mapped RX J1347−1145 at 150 GHz with the NOBA/NRO instrument. They get a 2′ × 2′ map of the cluster center. To compare our work to theirs, we have divided the center of our map in the same four regions as they did (50″ × 50″ square; southeast, northeast, northwest, and southwest). We have integrated the flux in each region. The value derived for each region can then be compared to that extracted from the NOBA/

NRO map. The results are presented in Table 2. We also show the integrated values for our residual map. We do not confirm the negative excess for the southeast quadrant. Instead, our measurement is symmetrical within the noise level. If any departure is to be searched in our map, then it is a positive excess in the southwest quadrant, of 2.8 ± 1.4. Despite the low significance level of this excess and referring to our residual map, we suggest that this excess is compatible with the presence of a second point source in this region. This hypothesis is supported by the point source detected at 350 GHz with SCUBA and at 8.46 GHz with the VLA by Komatsu et al. (2000, private communication). Its VLA position is $\alpha_{2000} = 13^{h}47^{m}27^{s}.72$, $\delta_{2000} = -11°45'52''.86$. The SCUBA and VLA fluxes are 17.9 ± 4.8 and 0.490 ± 0.043 mJy, respectively. This source seems to be an infrared source. A millimeter residual, provided by the millimeter tail of a dust emission, could contribute to our signal. Complementary millimeter observations are needed for this source.

4.2. *The Gas Mass Profile*

From the Diabolo map, we can directly estimate the gas mass that gives rise to the measured SZ signal. The SZ signal can be directly converted into a gas mass value by applying the linear transformation $M(\theta) = CF_{\nu}(\theta)$, where C is a constant that depends on the redshift ($z = 0.45$) and also on the gas temperature. The SZ signal map is obtained after the subtraction of the point-source best-fit model (see § 4.1). This RX J1347−1145 SZ map is shown in Figure 1*c* (the X-ray contours have been overplotted). Afterward, it is converted into a gas mass map, which is then integrated with respect to the distance to the cluster center (see Fig. 3).

Because of the size of the Diabolo map and especially the part used to subtract the baseline (30% on the edge of each line), we could only measure the projected gas mass within a projected radius of 74″ (i.e., 0.6 Mpc): $M_{\rm gas}^{\rm SZ}(\theta < 74'') = (1.1 \pm 0.1) \times 10^{14}\, h_{50}^{-5/2}\, M_{\odot}$. The error bar are quoted at a 68% confidence level. This value agrees very well with the estimated gas mass derived from the X-ray best-fit model (under the hypothesis of a spherical β-model): $M_{\rm gas}^{\beta\text{-model}}(r < 0.6\ {\rm Mpc}) = 10^{14}\, h^{-5/2}\, M_{\odot}$.

This result confirms the agreement of the SZ and X-ray data, when the hypothesis of the β-model is adopted. In our case, no bias has been introduced in the measured projected mass by the baseline subtraction. In fact, the part of each line used to subtract the baseline has been taken out of 0.6 Mpc from the cluster center. A radius of 0.6 Mpc corresponds to an angular radius of 74″.2 ($8.8r_c$). Assuming a virial radius of $10r_c$, the mass unaccounted for is estimated as no more than 16% of the total gas mass.

TABLE 2

FLUXES IN 50″ × 50″ REGIONS AS DEFINED BY KOMATSU ET AL. (2000)

Region (1)	Map (mJy) (2)	Residual Map (mJy) (3)	NOBA/NRO (mJy) (4)
Southeast	−12.2	−0.8	−11.3
Northeast	−9.9	−0.7	−4.7
Northwest.....	−10.1	−0.4	−3.3
Southwest.....	−6.8	2.8	−6.1
1 σ noise	1.4	1.4	2.0

NOTE.—Col. (2): Diabolo fluxes; col. (3): residual flux after the subtraction of the best fit model; col. (4): NOBA/NRO fluxes. Cols. (2) and (4) should be compared. The second column tries to highlight some eventual excess (positive or negative). For each column, the associated 1 σ noise flux is quoted.

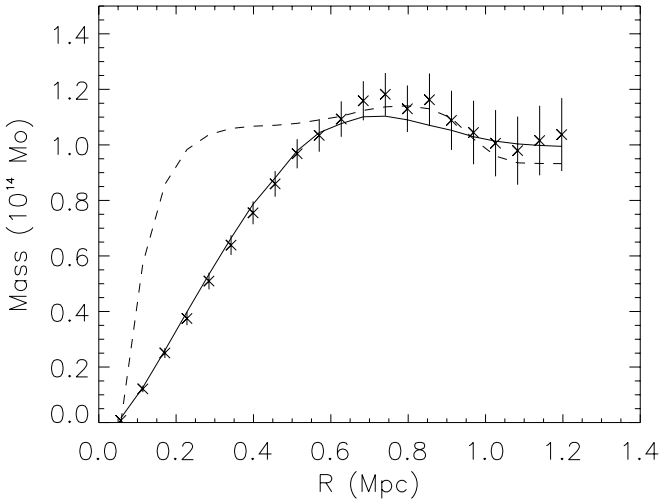

FIG. 3.—RX J1347−1145 gas mass profile computed directly from the 2.1 mm map. The solid line represents the gas mass profile of the SZ best-fit model. The integral of the Diabolo beam (*dashed line*) has been overplotted and scaled to the gas mass profile to show the extension of the SZ signal.

Our determination of the gas mass agrees with the X-ray determination. However, the X-ray total mass determination disagree with the strong-lensing (Sahu et al. 1998) and weak-lensing (Fischer & Tyson 1997) determinations by a factor of 2. Allen (1998) explained this discrepancy by the effect of the cooling flow on the total mass estimation using X-ray data. He concludes that the correction from this effect removes the differences between the estimators of the total mass. As an example, we can propose an increase of the gas temperature by a factor of 2 ($\sim$18 keV). To keep the SZ signal unchanged, this increase must be balanced by a decrease of the gas density by a factor of 2. It then affects our results in the following ways: (1) The inferred total mass will be divided by a factor of 2 [$M_{\rm gas}(r < 0.6\ {\rm Mpc}) = (0.61 \pm 0.04) \times 10^{14}\, h_{50}^{-5/2}\, M_{\odot}$]. The total mass will also increase by a factor of 2 and then be in agreement with the lensing measurements. (2) As long as we suggest an increase of the gas temperature balanced by a decrease of the gas density, the SZ signal will remain unchanged. On the other hand, the X-ray flux will decrease by more than a factor of 2 [scaling the X-ray flux as $n_e(0)^2(T_g)^{1/2}$]. Consequently, the Hubble constant will be affect by a factor of 2 ($H_0 \propto F_{\rm SZ}^2/F_{\rm X}$).

The previous scheme is very simple. The thermodynamic state of the intracluster medium is probably more complex, mainly made of two gas components. A cold ($\propto$9 keV), dense, and peaked central component surrounded by a hot ($\propto$18 keV), thin, and extended component. In this case, the cluster should present a nonisothermal radial profile (assuming the spherical symmetry). This kind of hypothesis could explain the very strong degeneracy that we encountered while trying to determine the core radius (see § 4.1). Unfortunately, the quality of our data is not good enough to argue in this direction. Nevertheless, this suggestion is not unlikely. Recent *XMM-Newton* observations have already shown such a behavior in other cooling-flow clusters, such as A1795 (Arnaud et al. 2001; Tamura et al. 2001) and A1835 (Peterson et al. 2001)

4.3. *Point Sources*

The best-fit model gives a flux of 5.7 ± 1.5 mJy beam^{-1} for the central point source. This point source can be visualized on the data map after the subtraction of the SZ component. Figure 1*d* clearly shows an excess of positive emission in its center. The NVSS map (Condon et al. 1998) has been overplotted as contours. Both signals match very well in term of position.

This point source has already been observed at different frequencies. It has been detected in the NVSS by Condon et al. (1998) with a flux of 46.9 ± 1.9 mJy at 1.4 GHz. Komatsu et al. (1999) have reported various measurements of this point source: an OVRO flux of 10.1 ± 0.5 at 28.5 GHz, a Nobeyama Millimeter Array (NMA) flux of 5 ± 1.5 mJy at 100 GHz, and a 2 σ upper limit of 4.8 mJy obtained with SCUBA at 350 GHz. From this set of measurements and assuming a power-law spectrum for the point-source radio emission, they have derived $F_{\rm RS} = (55.7 \pm 1.0)\nu_{\rm GHz}^{-0.47\pm0.02}$ mJy. More recently, Komatsu et al. (2001) have observed it with the VLA at 8.46 and 22.46 GHz. The respective detected flux are 22.42 ± 0.04 and 11.5 ± 0.17 mJy.

Using those latest measurements, we update the point-source power spectrum determination: $F_{\rm RS} = (77.8 \pm 1.7)\nu_{\rm GHz}^{-0.58\pm0.01}$ mJy. The quality of this fit is moderate, because of the very robust constraints given by some of the data points (see Fig. 4). It is difficult to conclude firmly that a single power spectrum can correctly model the synchrotron emission from radio down to millimeter wavelengths. The intensity and spectral shape of the synchrotron emission are driven by the internal magnetic field of the radio source. Furthermore, its strength also drives the maximum frequency of emission allowed. To date, many radio sources have been observed with various intensity and spectral shapes. Because of this high rate of variation from one source to an other and because of the lack of millimeter data, we are not able to state an eventual cutoff in the spectral shape of our radio source. For this reason, we adopted the previously defined power-law model. It provides us an estimation of the flux contributed by the central point source at 143 GHz (2.1 mm).

To explain the nature of the millimeter emission we have detected, we now compare the residual radio flux expected at 143 GHz (2.1 mm) and 350 GHz (850 μm) from the previous power-law spectrum to the flux obtained from the Diabolo and SCUBA data, respectively. At 2.1 mm, we have extrapolated $F_{\rm RS}^{\rm est}(2.1\ {\rm mm}) = 4.3 \pm 0.3$ mJy. This estimation is at 1 σ, compatible with our determination from the Diabolo map. The 350 GHz (e.g., 805 μm) flux can be estimated as well, at $F_{\rm RS}^{\rm est}(0.85\ {\rm mm}) = 2.7 \pm 0.4$ mJy. Now, from the SCUBA data points published by Komatsu et al. (1999), we have subtracted the positive SZ contribution, computed from the cluster SZ spectrum and scaled by our y best-fit value. The SZ radial profile has been obtained from model C (see § 4.1) convolved with the SCUBA beam (a Gaussian beam with $\sigma_{\rm FWHM} = 15''$). We fixed the value of the signal offset (so-called DC offset) to 2.7 mJy beam^{-1} as published by Komatsu et al. We finally deduced for the point source $F_{\rm RS}(0.85\ {\rm mm}) = 1.8 \pm 1.0$ mJy. The low signal-to-noise ratio of this last flux does not allow us to consider this result as the detection of a real submillimeter point source.

Nevertheless, our Diabolo flux and the SCUBA flux are both compatible with the estimation extrapolated from the point-source power spectrum. For this reason, it seems reasonable to deduce that the point-source emission seen in our map is likely due to the synchrotron millimeter tail of the central radio point source emission.

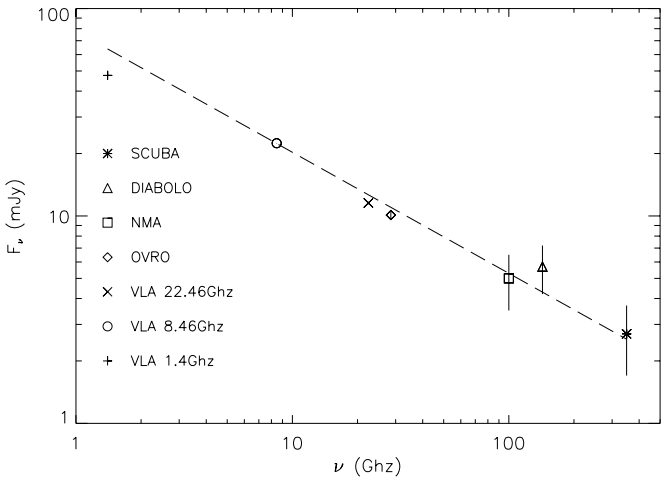

FIG. 4.—Central point-source spectrum from 1.4 to 350 GHz

5. CONCLUSION

We have produced an extended map ($4' \times 4'$) of the RX J1347−1145 cluster with the Diabolo photometer. We have drawn the distribution of the SZ signal up to 74″ (0.6 Mpc) from the cluster center. This SZ signal is as much extended as the X-ray emission and is the strongest SZ effect detected to date.

The SZ map allows us to directly derive the projected mass distribution and to measure the cluster gas mass up to 0.6 Mpc. We derive $M_{\rm gas} = (1.1 \pm 0.1) \times 10^{14}\ h_{50}^{-5/2}\ M_\odot$. The gas mass estimated within the same region, under the assumption of a classical β-model and the cluster parameters derived from the X-ray data, agrees with our value.

As a consequence of the map noise level and the observing strategy, we are not able to firmly conclude the existence of substructure in the gas distribution. Nevertheless, our map presents some asymmetric features at more than a 2 σ level.

At the moment, the first results of the *Chandra* and *XMM-Newton* satellites, concerning the observation of galaxy clusters, already show some departure in the density distribution from the β-model symmetry, as well as in the temperature distribution from the isothermality (Fabian et al. 2000; Vikhlinin, Markevitch, & Murray 2000; Arnaud et al. 2001; Tamura et al. 2001; Peterson et al. 2001). For this reason, comparisons of the upcoming *Chandra* and *XMM-Newton* X-ray observations to actual and future SZ data (from interferometers and bolometer arrays) are needed to understand the cluster physical structure.

The authors want to thanks the IRAM staff (from astronomers to cookers). Thanks to N. Aghanim, E. Komatsu, M. Hattori, and Y. Suto for their fruitful comments and discussions. We are very grateful to the anonymous referee for the quality of his report, which helped us to improved and clarify our paper. Diabolo is supported by the Programme National de Cosmologie, Institut National pour les Sciences de l'Univers, Ministère de l'Education Nationale de l'Enseignement Supérieur et de la Recherche, CESR, CRTBT, IAS-Orsay, and LAOG.

REFERENCES

Allen, S. W. 1998, MNRAS, 296, 392
Arnaud, M. et al. 2001, A&A, 365, L67
Benoit, A., et al. 2000, A&AS, 141, 523
Bahcall, N. A., & Fan, X. 1998, ApJ, 504, 1
Birkinshaw, M. 1999, Phys. Rep., 310, 97
Cavaliere, A., & Fusco-Femiano, R. 1976, A&A, 49, 137
Condon, J. J., Cotton, W. D., Greisen, E. W., Yin, Q. F., Perley, R. A., Taylor, G. B., & Broderick, J. J. 1998, AJ, 115, 1693
Désert, F. X., et al. 1998, NewA, 3, 655
Fabian, A. C., et al. 2000, MNRAS, 318, 65L
Fischer, P., & Tyson, J. A. 1997, AJ, 114, 14
Komatsu, E., Kitayama, T., Suto, Y., Hattori, M., Kawabe, R., Matsuo, H., Schindler, S., & Yoshikawa, K. 1999, ApJ, 516, L1
Komatsu, E., et al. 2001, PASJ, 53, 57
Oukbir, J., Bartlett, J. G., & Blanchard, A. 1997, A&A, 320, 365
Peterson, J. R., et al. 2001, A&A, 365, L104
Pointecouteau, E., Giard, M., & Barret, D. 1998, A&A, 336, 44
Pointecouteau, E., Giard, M., Benoit, A., Désert, F. X., Aghanim, N., Coron, N., Lamarre, J. M., & Delabrouille, J. 1999, ApJ, 519, L115
Sadat, R., Blanchard, A., & Oukbir, J. 1998, A&A, 329, 21
Sahu, K. C., et al. 1998, ApJ, 492, L125
Schindler, S., Hattori, M., Neumann, D. M., & Boehringer, H. 1997, A&A, 317, 646
Schindler, S., et al. 1995, A&A, 299, L9
Sunyaev, R., & Zeldovich, Y. 1972, Comments Astrophys. Space Phys., 4, 173
Tamura, T., et al. 2001, A&A, 365, L87
Vikhlinin, A., Markevitch, M., & Murray, S. S. 2000, ApJ, submitted (preprint astro-ph/0008496)